The Plant Cell, Vol. 25: 4544–4559, November 2013, www.plantcell.org © 2013 American Society of Plant Biologists. All rights reserved.

The Actin-Related Protein2/3 Complex Regulates Mitochondrial-Associated Calcium Signaling during Salt Stress in *Arabidopsis*[C][W]

Yi Zhao,[a,1] Zhen Pan,[a,b,1] Yan Zhang,[a] Xiaolu Qu,[c] Yuguo Zhang,[a] Yongqing Yang,[a] Xiangning Jiang,[b,d] Shanjin Huang,[c] Ming Yuan,[a] Karen S. Schumaker,[e] and Yan Guo[a,f,2]

[a] State Key Laboratory of Plant Physiology and Biochemistry, College of Biological Sciences, China Agricultural University, Beijing 100193, China

[b] College of Life Sciences and Biotechnology, Beijing Forestry University, Beijing 100083, China

[c] Key Laboratory of Plant Molecular Physiology, Institute of Botany, Chinese Academy of Sciences, Beijing 100093, China

[d] National Engineering Laboratory of Tree Breeding, The Tree and Ornamental Plant Breeding and Biotechnology Laboratory of State Forestry Administration, Beijing 100083, China

[e] School of Plant Sciences, University of Arizona, Tucson, Arizona 85721

[f] National Center for Plant Gene Research, Beijing 100193, China

Microfilament and Ca^{2+} dynamics play important roles in stress signaling in plants. Through genetic screening of *Arabidopsis thaliana* mutants that are defective in stress-induced increases in cytosolic Ca^{2+} ($[Ca^{2+}]_{cyt}$), we identified Actin-Related Protein2 (Arp2) as a regulator of $[Ca^{2+}]_{cyt}$ in response to salt stress. Plants lacking Arp2 or other proteins in the Arp2/3 complex exhibited enhanced salt-induced increases in $[Ca^{2+}]_{cyt}$, decreased mitochondria movement, and hypersensitivity to salt. In addition, mitochondria aggregated, the mitochondrial permeability transition pore opened, and mitochondrial membrane potential Ψm was impaired in the *arp2* mutant, and these changes were associated with salt-induced cell death. When opening of the enhanced mitochondrial permeability transition pore was blocked or increases in $[Ca^{2+}]_{cyt}$ were prevented, the salt-sensitive phenotype of the *arp2* mutant was partially rescued. These results indicate that the Arp2/3 complex regulates mitochondrial-dependent Ca^{2+} signaling in response to salt stress.

INTRODUCTION

Ca^{2+} is a universal second messenger, regulating cellular responses to environmental changes in plants. Many abiotic stresses, including soil salinity (salt stress), drought, cold, oxidative stress, and wounding cause transient increases in cytosolic-free Ca^{2+} levels ($[Ca^{2+}]_{cyt}$) (Knight et al., 1991; Knight et al., 1996, 1997; Frohnmeyer et al., 1999; Rentel and Knight, 2004). The increase in $[Ca^{2+}]_{cyt}$ is due to the release of the ion from internal and external (apoplastic) Ca^{2+} stores and often varies in pattern (e.g., oscillations or spikes). Precise regulation of proteins that transport Ca^{2+} (channels, pumps, and carriers) and proteins that bind to Ca^{2+} (binding proteins and sensors) leads to regulation of cellular Ca^{2+} ion homeostasis (Berridge et al., 2003). Changes in the duration, amplitude, and frequency of $[Ca^{2+}]_{cyt}$ underlie its specificity in signaling.

An important strategy for plant adaptation to growth in saline environments involves regulation of cellular sodium ion homeostasis to reduce the buildup of toxic levels of sodium in the plant. This Ca^{2+}-dependent process was first demonstrated in *Arabidopsis thaliana* by the isolation of mutants with increased salt sensitivity (*salt overly sensitive* [*sos*]) relative to wild-type plants (Zhu et al., 1998). Cloning of the genes altered in these mutants and characterization of their protein products led to the identification of the SOS pathway. SOS pathway components include SOS3, a Ca^{2+} binding protein (Liu and Zhu, 1998; Liu et al., 2000) that responds to increases in $[Ca^{2+}]_{cyt}$ and activates SOS2, a Ser/Thr protein kinase (Liu et al., 2000). Activated SOS2 regulates the activity of the SOS1 Na^+/H^+ exchanger in the plasma membrane to transport sodium out of the cell (Ishitani et al., 2000; Shi et al., 2000; Guo et al., 2001; Qiu et al., 2002, 2003).

One output of the SOS pathway is regulation of actin microfilament (MF) dynamics and stability (Wang et al., 2010; Zhou et al., 2010; Liu and Guo, 2011; Ye et al., 2013). MFs in both the *sos2* and *sos3* mutants have abnormal dynamics and depolymerize faster than in the wild type (Wang et al., 2010; Ye et al., 2013). More recently, MF dynamics modulated by the Actin-Related Protein2 Arp2/3 complex were reported to regulate stomatal movement, and a change in calcium signaling was hypothesized to play a key role in this response (Jiang et al., 2012). The Arp2/3 complex contains seven components (Arp2, Arp3, and Arpc1-5) and is evolutionarily conserved in yeast, plants, and animals (Deeks and Hussey, 2005; Yanagisawa et al., 2013). This actin nucleator complex is required for cell motility and membrane trafficking (Goley and Welch, 2006). In

[1] These authors contributed equally to this work.

[2] Address correspondence to guoyan@cau.edu.cn.

The author responsible for distribution of materials integral to the findings presented in this article in accordance with the policy described in the Instructions for Authors (www.plantcell.org) is: Yan Guo (guoyan@cau.edu.cn).

[C] Some figures in this article are displayed in color online but in black and white in the print edition.

[W] Online version contains Web-only data.

www.plantcell.org/cgi/doi/10.1105/tpc.113.117887

Arabidopsis, mutations in Arp2/3 complex components lead to disordered MF bundles that result in defective epidermal cell expansion in trichomes, root hairs, hypocotyls, and leaves (Mathur, 2005; Szymanski, 2005). The Arp2/3 complex is also involved in the regulation of light-induced root elongation (Dyachok et al., 2008, 2011).

Mitochondria play key roles in the maintenance of Ca^{2+} ion homeostasis (Vandecasteele et al., 2001), and studies have shown that MF dynamics are important for the arrangement, distribution, and function of mitochondria (Vandecasteele et al., 2001). Mitochondria move along MFs and function as Ca^{2+} stores in plant cells (Vandecasteele et al., 2001; Wang et al., 2004a), and stress induces mitochondrial-mediated cell death processes in plants (Yao et al., 2004; Lin et al., 2005; Gao et al., 2008). It has been shown that actin is present in mung bean (*Vigna radiata*) mitochondria (Lo et al., 2011) and that two glycolytic enzymes in *Arabidopsis* interact with mitochondrial VOLTAGE-DEPENDENT ANION CHANNEL3 and bind to F-actin (Wojtera-Kwiczor et al., 2012), suggesting that mitochondria directly associate with F-actin.

The mitochondrion acts as a sensor of death signals and an initiator of the biochemical processes that lead to the controlled destruction of the cell (Green and Kroemer, 2004). When cells enter programmed cell death, the mitochondrial permeability transition pore (mPTP) opens and mitochondrial membrane potential Ψm (MTP) decreases. In animals and plants, an irreversible opening of the mPTP at high conductance usually takes place before mitochondrial-mediated cell death and serves to release cell death factors, including cytochrome *c* (Yang et al., 1997; Balk et al., 1999).

Although mitochondrial-mediated Ca^{2+} signaling has been identified in plants, the molecular mechanisms underlying this process have not been identified, and little is known about how a specific Ca^{2+} signature is generated. Based on a forward-genetic screen, we demonstrate that the Arp2/3 complex is involved in a salt-induced, mitochondrial-dependent increase in $[Ca^{2+}]_{cyt}$ that is critical for plant salt tolerance.

RESULTS

The *1648* Mutant Has Enhanced Salt Stress–Induced $[Ca^{2+}]_{cyt}$ and Decreased Salt Tolerance

To identify components that regulate $[Ca^{2+}]_{cyt}$ in response to salt stress, the *AEQUORIN* reporter gene (Knight et al., 1991), driven by the cauliflower mosaic virus 35S promoter, was transformed to *Arabidopsis* ecotype Columbia-0 (Col-0). This constitutively expressing *35S:AEQUORIN* line was used as the wild type in this study, and a T-DNA insertional mutant pool was constructed based on this wild type (Zhao et al., 2001, 2011; Zheng et al., 2012). We screened for mutants with altered $[Ca^{2+}]_{cyt}$ when plants were treated with NaCl. For screening, 7-d-old seedlings were left untreated or treated with 200 mM NaCl, and luminescence was measured immediately with a cold charge-coupled device (CCD) imaging system. Several mutants were isolated; one of these, *1648*, displayed an enhanced increase in $[Ca^{2+}]_{cyt}$ (Figure 1A). The value for $[Ca^{2+}]_{cyt}$ in the mutant before treatment was similar to the wild type and was in an undetectable level. However, the salt-stimulated increase was dramatically higher with peak values as high as 1 ± 0.15 μM compared with 0.5 ± 0.1 μM in the wild type (Figure 1B).

To determine if this enhanced $[Ca^{2+}]_{cyt}$ affected the response of the mutant to salt, 5-d-old *1648* and wild-type seedlings grown on Murashige and Skoog (MS) medium were transferred to MS without or supplemented with 100, 150, or 200 mM NaCl for phenotypic analysis. Without salt, the length of branch roots in the mutant was slightly longer than in the wild type, and on low levels of salt (100 mM), the mutant showed a slight increase in sensitivity (Figures 1C and 1D). When plants were transferred to medium containing 150 or 200 mM NaCl, the leaves of the mutant were bleached by the fourth day of treatment (Figure 1C), and the percentage of mutant seedlings that survived was significantly lower than in the wild type during salt stress (Figure 1D). To determine if salt caused differential damage to cellular integrity, electrolyte leakage was measured in the wild type and mutant after treatment with 150 mM NaCl. The results indicate that the plasma membrane in root cells of the mutant was more severely damaged than in the wild type (Figure 1E). The hypersensitivity to salt seen in the mutant represented an ionic and not an osmotic effect as the mutant was specifically sensitive to Na^+ (Figure 1C), K^+, Li^+, and Cs^+ but not to polyethylene glycol (see Supplemental Figure 1 online). Consistent with this observation, the value for $[Ca^{2+}]_{cyt}$ was similar to the wild type in the 10-d-old mutant seedlings after 200 mM mannitol treatment (see Supplemental Figure 1 online).

The Arp2/3 Complex Functions during Salt Stress and Ca^{2+} Signaling in *Arabidopsis*

Using simple sequence length polymorphism markers, we mapped the *1648* locus to chromosome III between MQP17 and MYF5 (Bacterial Artificial Chromosome clones of The Arabidopsis Information Resource) within ~73 kb. We then sequenced all of the coding sequences (CDSs) in this region. A 4-bp deletion and a single nucleotide substitution (C to T) in exon 6 were identified in At3g27000 (encoding Arp2). This mutation was located 721 bp downstream of the *Arp2* translation initiation codon and introduced a frame shift and a premature stop codon in the *Arp2* CDS (Figure 2). Thus, we renamed this mutant *arp2-2*.

The Arp2/3 complex is the primary nucleation factor of new actin filaments in most organisms. Previous studies have shown that a mutation in *Arp2* (*arp2-1*) resulted in abnormal trichome formation in *Arabidopsis* (Mathur et al., 1999). As expected, the distorted trichome defect was also observed in *arp2-2* (the trichome stalk was disordered and branch lengths were reduced; Figure 3A), and hypersensitivity to salt was also observed in the original *arp2-1* mutant (Figures 3C and 3D). To provide additional support that the phenotypes in *arp2-2* are due to the disruption of *Arp2*, we complemented the *arp2-2* mutant phenotype with the *Arp2* cDNA expressed under the control of the native *Arp2* promoter (including a 1.5-kb fragment upstream of the start of translation). Eight independent transgenic lines complemented the trichome defect phenotype of the *arp2-2* mutant in T3 homozygous plants; one of them, complementation line8 (com8), is shown in Figure 3. We then analyzed the

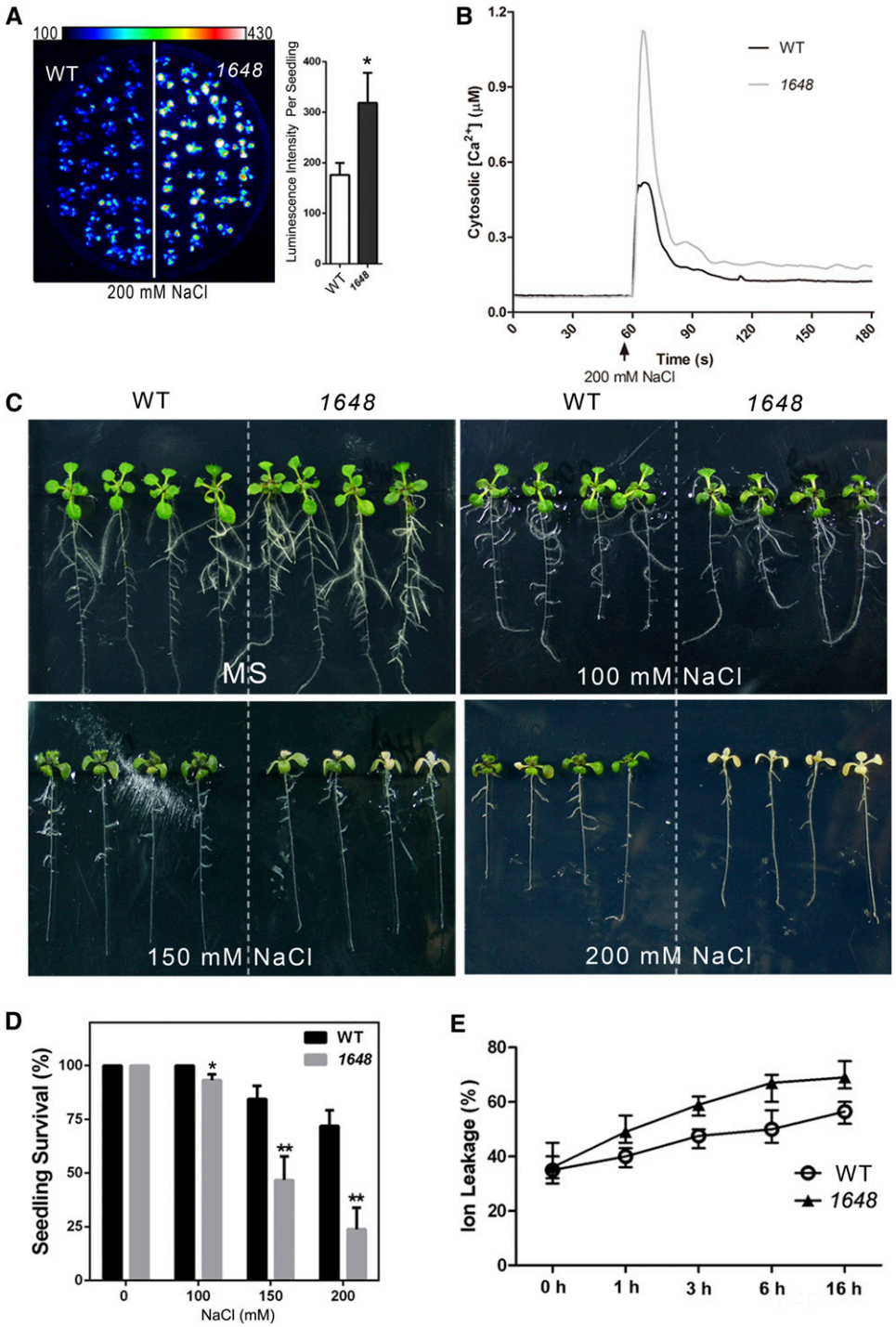

Figure 1. The *1648* Mutant Displays NaCl-Induced Increase in $[Ca^{2+}]_{cyt}$ Concentration and Salt Sensitivity.

(A) Pseudocolor luminescence images of Ca^{2+}-dependent photons emitted by aequorin wild-type (WT) and *1648* seedlings treated with 200 mM NaCl. The mean luminescence value for wild-type and *1648* single seedlings over a 180-s integration period is shown in the graphs to the right of each image. Data represent means ± SD; $n = 60$. Asterisks indicate a significant difference (*$P < 0.05$; Student's t test) between the mutant and the wild type for the same treatment.

(B) Time course of $[Ca^{2+}]_{cyt}$ signaling in 10-d-old wild-type and *1648* seedlings in response to treatment with 200 mM NaCl (arrow). The data show one representative image of five independent experiments.

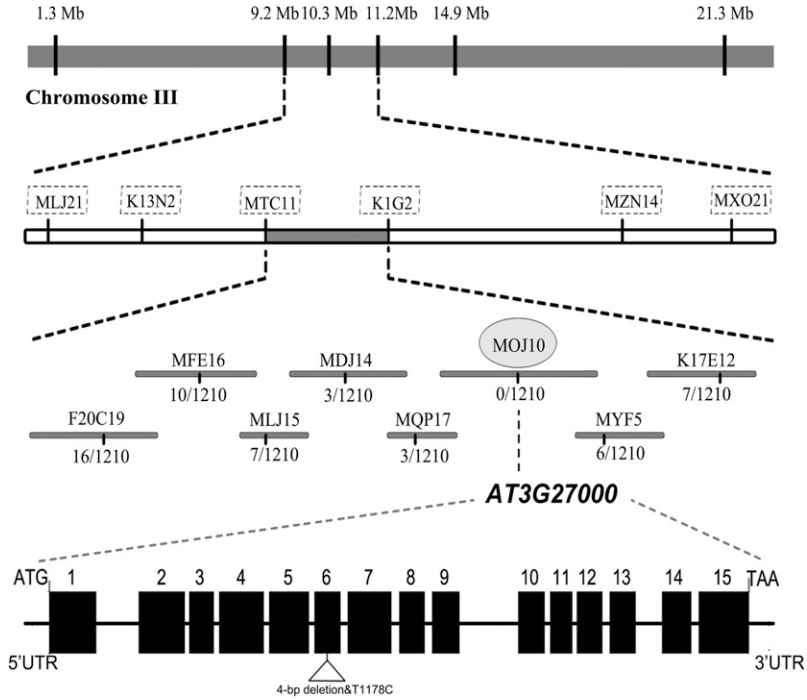

Figure 2. Map-Based Cloning of *1648*.

The mutation in *1648* maps to the *Arp2* gene. Exons are shown as black boxes, and introns are shown as lines. UTR, untranslated region.

Ca^{2+} response of com8 treated with salt and found that the Ca^{2+} signal in com8 was reduced to the same level as in the wild type (Figure 3B).

Because the *Arabidopsis* Arp2/3 complex contains seven members, we tested the responses of *arpc5* and *arpc2a*, containing mutations in two additional complex members, and found that they also showed the *arp2*-like salt-sensitive phenotype (Figure 3C; see Supplemental Figure 2 online). When we crossed the *35S:AEQUORIN* transgene into *arp2-1*, *arpc2*, and *arpc5*, all mutants displayed enhanced $[Ca^{2+}]_{cyt}$ when stimulated with salt (see Supplemental Figures 3A and 3B online). These data indicate that the Arp2/3 complex functions during salt stress and Ca^{2+} signaling in *Arabidopsis*.

Because the Arp2/3 complex plays important roles in MF organization (Machesky and Gould, 1999), we monitored MFs before and after salt treatment in *arp2-2* and the wild type. For these studies, we transformed *Pro35S:fABD2-GFP* (for expression of the second actin binding domain of *Arabidopsis* FIMBRIN1 fused to green fluorescent protein) (Wang et al., 2004b) into the wild type and *arp2-2*. The actin cytoskeleton was visualized directly in both cotyledon pavement cells and hypocotyl cells. Before salt treatment, no obvious difference in actin organization in cotyledon pavement cells was detected in *arp2-2* when compared with actin organization in the wild type. However, MF density was lower in *arp2-2* than in wild-type seedlings before and after salt treatment (Figures 4A and 4D), suggesting

Figure 1. (continued).

(C) Salt sensitivity of wild-type and *1648* seedlings. Five-day-old wild-type and *1648* seedlings were transferred from solid MS medium to solid MS medium without or with 100, 150, or 200 mM NaCl. Photographs were taken 4 d after transfer.

(D) Seedling survival for wild-type and *1648* seedlings treated with salt. Five-day-old wild-type and *1648* seedlings were transferred from solid MS medium to solid MS medium without or with 100, 150, or 200 mM NaCl. Survival (green cotyledons and rosette leaves) was measured 4 d after transfer. Data represent means ± SD; $n > 30$. Asterisks indicate a significant difference (*$P < 0.05$ and **$P < 0.01$; Student's *t* test) between the mutant and the wild type for the same treatment.

(E) Ion leakage in wild-type and *1648* seedlings. Seven-day-old seedlings grown on solid MS plates were transferred to solid MS media containing 150 mM NaCl. After 24 h, seedlings were removed from plates, washed with deionized water, and placed in tubes containing 5 mL of deionized water. The tubes were shaken overnight, and the conductivity of the solution was measured using a conductivity meter. Tubes containing the seedlings were then autoclaved and, after the tubes cooled to room temperature, conductivities of the solutions were remeasured. The percentage of electrolyte leakage was calculated as a ratio of the conductivity before and after autoclaving. Data represent means ± SD; $n = 3$ for each treatment.

[See online article for color version of this figure.]

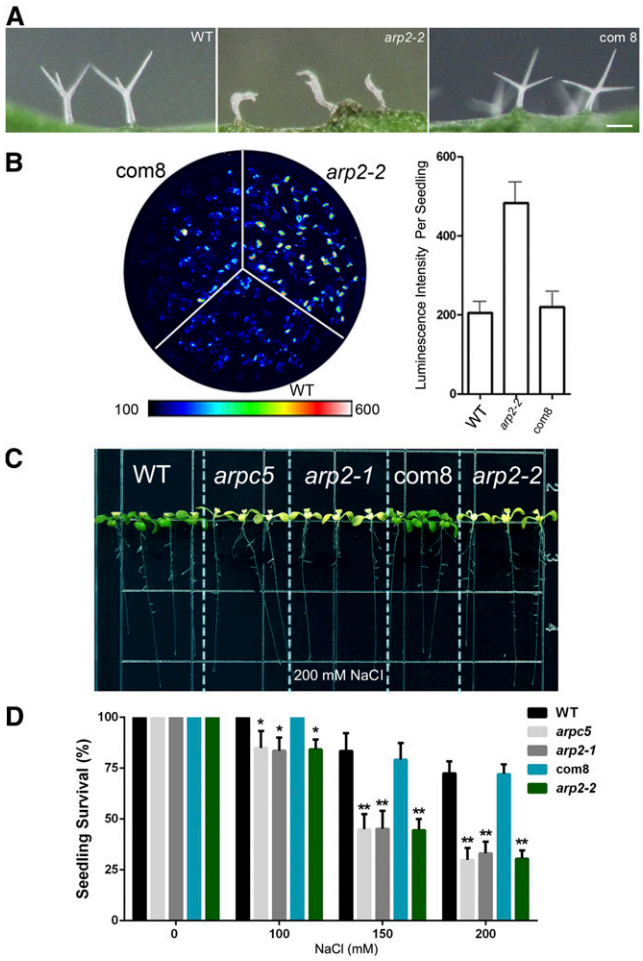

Figure 3. Verification of Phenotypes Found in Mutants of *Arabidopsis* Arp2/3 Complex Genes.

(A) Comparison of trichomes in the wild type (WT), *arp2-2*, and com8, a complemented *arp2-2* mutant line. Images show leaves of 7-d-old seedlings.

(B) Salt-induced increases in $[Ca^{2+}]_{cyt}$ in com8. Salt-induced increases in $[Ca^{2+}]_{cyt}$ in the wild type, *arp2-2*, and com8 were measured with a CCD camera after treatment with 150 mM NaCl. The mean luminescence values of single seedlings are shown in the graphs to the right of the image. Data represent means ± SD for three independent experiments with 60 seedlings analyzed in each experiment.

(C) Salt sensitivity of the wild type and com8. Five-day-old seedlings of the wild type, com8, *arp2-1*, *arp2-2*, and *arpc5* were transferred from solid MS media to solid MS media with 200 mM NaCl. Photographs were taken 4 d after transfer and show one representative image of three independent replications.

(D) Seedling survival for com8 treated with salt. Five-day-old wild-type, com8, *arp2-1*, *arp2-2*, and *arpc5* seedlings were transferred from solid MS medium to solid MS medium without or with 100, 150, or 200 mM NaCl. Survival (green cotyledons and rosette leaves) was measured 4 d after transfer. Data represent means ± SD; $n > 30$. Asterisks indicate a significant difference (*$P < 0.05$ and **$P < 0.01$; Student's t test) between the mutant and the wild type for the same treatment.

that the Arp2/3 complex plays an important role in promoting actin assembly in cotyledon pavement cells. After treatment with 200 mM NaCl, actin filaments became depolymerized in *arp2-2* cotyledon pavement cells compared with control cells (Figures 4A and 4B). By contrast, most actin filaments remained intact in wild-type cotyledon pavement cells within the time window of NaCl treatment (Figures 4A and 4B), though actin filaments became more sparse during the later stages of the treatment (Figure 4A). To quantify the actin architecture in cotyledon pavement cells, two parameters, skewness (a measure of the degree of asymmetry of a distribution) and density (Higaki et al., 2010), were measured to evaluate the extent of actin filament bundling and the percentage of occupancy of actin filaments. Skewness increased significantly in *arp2-2* cotyledon pavement cells compared with skewness in wild-type cotyledon pavement cells 16 h after NaCl treatment (Figure 4C), suggesting that the extent of actin filament bundling increased after NaCl treatment in *arp2-2* cells. Additionally, a sustained decline of actin filament density in *arp2-2* cotyledon pavement cells was detected after treatment with 200 mM NaCl (Figure 4B). By contrast, no obvious reduction of actin filament density was detected in wild-type cotyledon pavement cells (Figure 4B), suggesting that Arp2/3-mediated actin assembly is required to balance NaCl-induced actin depolymerization. In hypocotyls, *arp2-2* cells had heavy actin filament bundles with much lower density than in the wild type (Figures 4E, 4G, and 4H), consistent with previous observations in trichomes (Le et al., 2003). The MFs in hypocotyl cells of the mutant were more sensitive to salt than MFs in the wild type, similar to what was seen in pavement cells, and the percentage of cells with depolymerized actin filaments increased with prolonged salt treatment (Figure 4F). Taken together, these data suggest that Arp2/3 complex–mediated actin assembly is involved in balancing salt-induced actin disassembly and maintaining the level of actin filaments during salt stress.

To confirm that the enhanced salt-induced $[Ca^{2+}]_{cyt}$ increase is due to the reduction of MFs, *arp2-2* and wild-type seedlings were pretreated with 1 μM Latrunculin B (Lat B; which binds monomeric actin and inhibits actin assembly). If MFs are important for regulating $[Ca^{2+}]_{cyt}$, the reduction of MFs in the wild type would be expected to result in an increase in $[Ca^{2+}]_{cyt}$. Results showed that the salt-induced $[Ca^{2+}]_{cyt}$ increase was higher in the wild type treated with Lat B than in control conditions, consistent with previous observations (Wang et al., 2004a). However, in *arp2-2*, Lat B treatment did not significantly affect the increase of $[Ca^{2+}]_{cyt}$ induced by 200 mM NaCl (see Supplemental Figure 4 online). These results indicate that depolymerization of MFs triggers changes in $[Ca^{2+}]_{cyt}$ and the Arp2/3 complex inhibits the increase of $[Ca^{2+}]_{cyt}$ under salt stress.

Arp2 Is Required for Mitochondrial Distribution

Because the Arp2/3 complex plays a role in MF-regulated maintenance of Ca^{2+} ion homeostasis and mitochondrial arrangement, distribution, and function require MF dynamics (Vandecasteele et al., 2001), we determined if the distribution of mitochondria is altered in the *arp2-2* mutant. For these experiments, we visualized mitochondria using MitoTracker Red

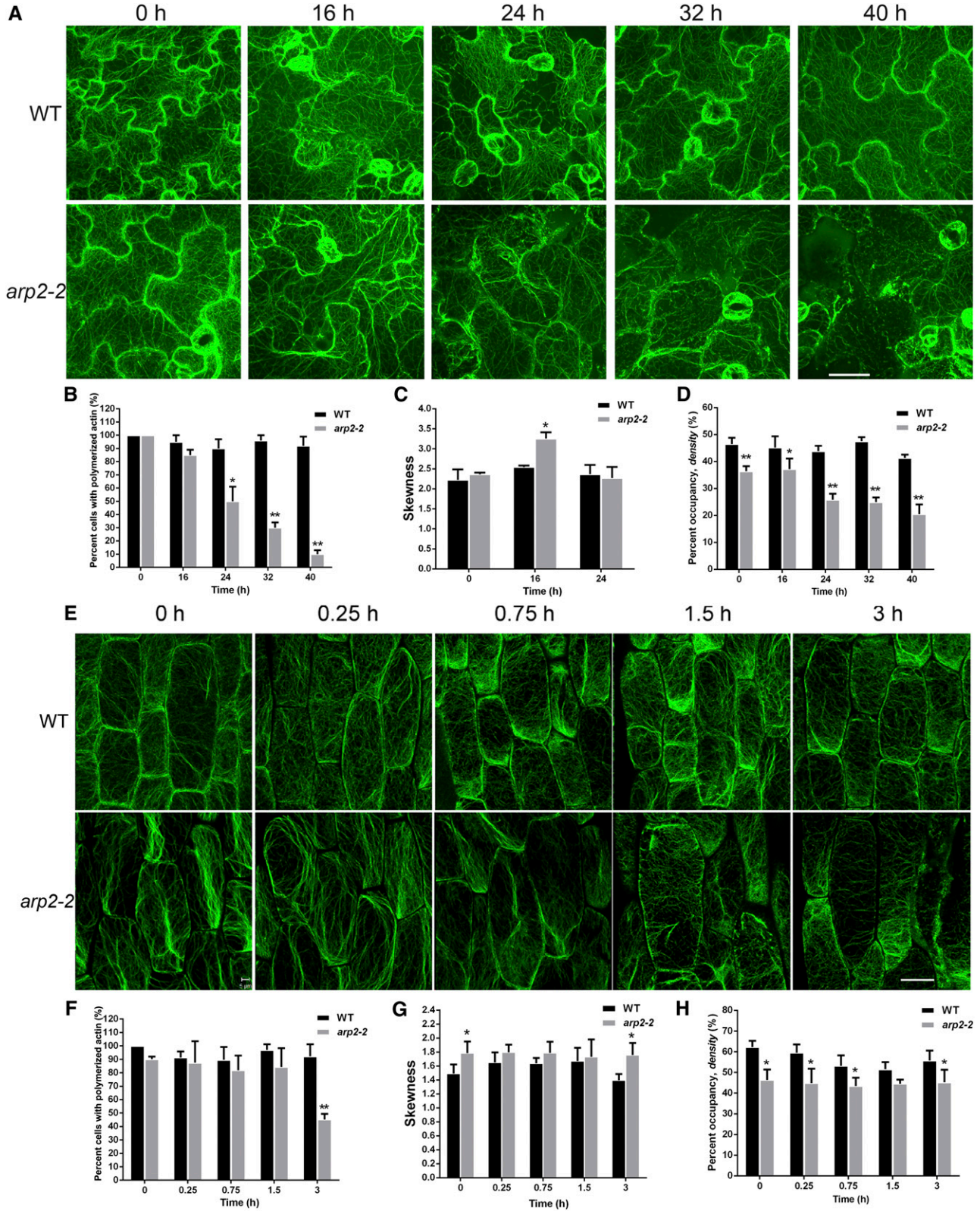

Figure 4. MF Organization Is Altered in *arp2-2* Cells during Salt Stress.

(A) MF organization of cotyledon pavement cells of the wild type (WT) and *arp2-2*. Seven-day-old seedlings of transgenic wild type or *arp2-2* harboring *Pro35S:fABD2-GFP* were treated with liquid MS media without or with 200 mM NaCl for the indicated times and seedlings were visualized with a confocal microscope. At least 10 independent leaves were analyzed in three experiments with similar results. Bar = 20 μm for all fluorescence images.

CMXRos (a mitochondrial-specific fluorescent dye) in *fABD2-GFP* transgenic plants and found that the mitochondrial distribution pattern was abnormal in *arp2-2*. Mitochondria tended to aggregate around thick MF bundles (Figure 5A). Zheng et al. (2009) reported that disruption of MFs by Latrunculin A– altered mitochondrial movement. Therefore, it is possible that the aggregation of mitochondria is due to impaired mitochondrial movement. To test this, we determined mitochondrial movement during salt treatments using spinning disk microscopy. Mitochondria associated with actin filaments in both the wild type and *arp2-2* (Figure 5B), suggesting that the association of this organelle with MFs does not rely on the Arp2/3 complex. We determined the velocity of mitochondrial movement and found that, in the wild type before NaCl treatment, mitochondria moved in the cortical cytoplasm at velocities ranging from 16 to 0.1 μm/s (Figure 5C) with an average velocity of 7.1 μm/s. In *arp2*-2, mitochondria moved in the cortical cytoplasm at velocities ranging from 12 to 0.1 μm/s (Figure 5C) with an average velocity of 3.0 μm/s. The average velocity in the mutant was substantially lower compared with that of the wild type, suggesting that the movement of mitochondria was impaired in *arp2-2*. After treatment with 150 mM NaCl, a decrease in mitochondrial movement was observed in both the wild type and *arp2-2* and became more significant with prolonged treatment. The percentage of mitochondria with velocities ranging from 0 to 2.0 μm/s (the slowest movement) increased more in *arp2-2* than in the wild type at different time points during NaCl treatment (Figure 5C). These data suggest that Arp2/3 complex–mediated actin dynamics are required for mitochondria movement and that the aggregation phenotype of mitochondria in *arp2-2* is very likely due to impaired mitochondria movement. Because it has been shown that the Arp2/3 complex is associated with multiple organelle surfaces (Kotchoni et al., 2009; Zhang et al., 2013), we determined whether the Arp2/3 complex directly associates with mitochondria. To do this, we generated *ProArp2:Arp2-MYC* transgenic plants in the *arp2-2* mutant background and found that normal trichome development was restored (Figure 3A), indicating that the construct is functional and can be used to determine the intracellular localization of Arp2. We next determined the localization of Arp2 (immune fluorescence probed with anti-MYC antibody) and mitochondria (costained with MitoTracker Red CMXRos) and found that Arp2 could likely colocalize with mitochondria (see Supplemental Figure 5 online). This implies that the Arp2/3 complex may promote actin assembly around mitochondria to contribute to mitochondrial movement.

Arp2 Regulates Mitochondrial Activity during Salt Stress

Mitochondrial activity is often associated with cell death. To determine if cell death is altered in mutants of the Arp2/3 complex after salt treatment, vital staining was performed. Five-day-old seedlings of the wild type, *arp2-2*, and *arpc5* were left untreated or treated with 150 mM NaCl for 24 h and then stained with trypan blue. Without salt treatment, no staining was detected in the cotyledon cells of the wild type, *arp2-2*, or *arpc5* (Figure 6A). After salt treatment, there was little staining in wild-type cotyledon cells, while significant numbers of *arp2-2* and *arpc5* cells were stained, suggesting that the salt sensitivity of the mutants is related, at least in part, to cell death (Figure 6B).

To determine if the mutation in *Arp2* affected mitochondrial activity, opening of the mPTP was determined in wild-type and *arp2-2* protoplasts during salt stress. mPTP opening was monitored using calcein/Co^{2+} imaging (Petronilli et al., 1999; Petronilli et al., 2001; Wang et al., 2010), and MitoTracker Red CMXRos was used to confirm that calcein was localized to the mitochondria (see Supplemental Figure 6A online). Protoplasts of the wild type and *arp2-2* were left untreated or treated with 150 mM NaCl for 10, 120, or 240 min. More than 100 protoplasts were counted for each sample, and the opening of the mPTP was indicated by a depletion of calcein fluorescence in the mitochondria. The results show that more cells with opened

Figure 4. (continued).

(B) Percentage of wild-type and *arp2-2* mutant cells with polymerized MF organization. Seven-day-old seedlings of transgenic wild-type and *arp2-2* plants expressing *Pro35S:fABD2-GFP* were treated with liquid MS media without or with 200 mM NaCl for the indicated times. With extended NaCl treatment, MFs in *arp2-2* became more unstable than in the wild type. Values represent means ± SE; $n > 50$. *$P < 0.05$ and **$P < 0.01$ by Student's *t* test.
(C) The extent of filament bundling (skewness) of pavement cells. Skewness in *arp2-2* was higher than in the wild type after 200 mM NaCl treatment for 16 h. Values represent mean ± SE; $n = 35$. *$P < 0.05$ by Student's *t* test.
(D) Average filament density of wild-type and *arp2-2* pavement cells. The filament density in *arp2-2* was less than in the wild type, and the actin filaments depolymerized after 200 mM NaCl treatment for 24 h or longer. Values represent mean ± SE; $n > 60$. *$P < 0.05$ and **$P < 0.01$ by Student's *t* test.
(E) MF organization of hypocotyl cells of the wild type and *arp2-2*. Seven-day-old seedlings of transgenic wild type or *arp2-2* expressing Pro*35S:fABD2-GFP* were treated with liquid MS media without or with 200 mM NaCl for the indicated times, and seedlings were visualized with a confocal microscope. At least 20 independent hypocotyls were analyzed in three experiments with similar results. Bar = 5 μm for all fluorescence images.
(F) Percentage of wild-type and *arp2-2* mutant hypocotyl cells with polymerized MF organization. Seven-day-old seedlings of transgenic plants expressing *Pro35S:fABD2-GFP* in the wild type and *arp2-2* mutant were treated with liquid MS media without or with 200 mM NaCl for the indicated times. When treatment time reached 3 h, MFs in *arp2-2* became more unstable than in the wild type. Values represent mean ± SE; $n > 80$. **$P < 0.01$ by Student's *t* test.
(G) The extent of filament bundling (skewness) of hypocotyl cells. Values represent mean ± SE; $n > 80$. *$P < 0.05$ by Student's *t* test.
(H) Average filament density of wild-type and *arp2-2* hypocotyl cells. The filament density in *arp2-2* was less than in the wild type, and the actin filaments depolymerized after 200 mM NaCl treatment for 24 h or longer. Values represent mean ± SE; $n > 80$. *$P < 0.05$ by Student's *t* test.
[See online article for color version of this figure.]

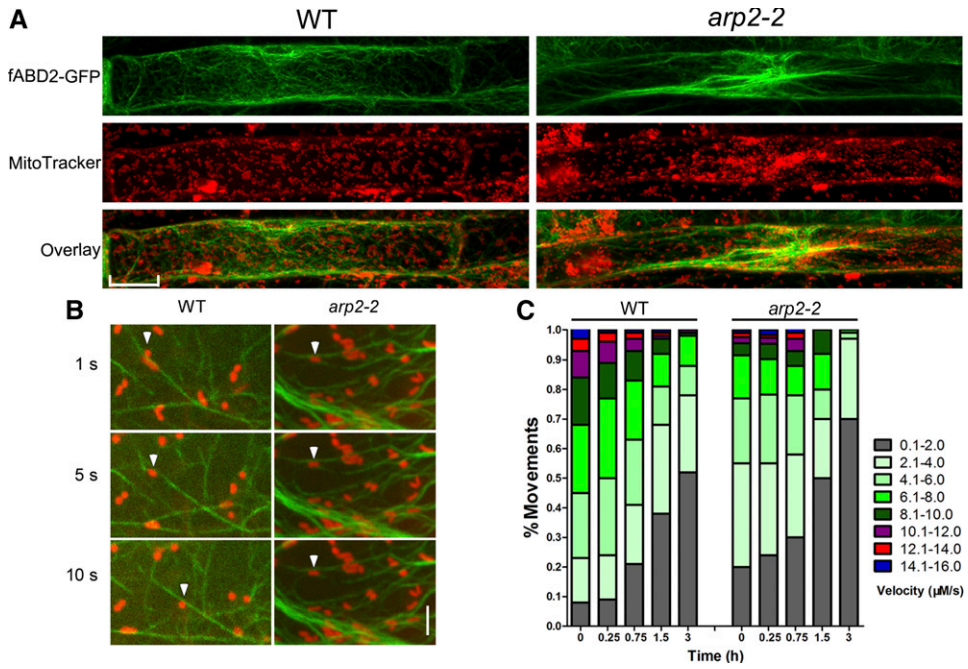

Figure 5. Mitochondrial Distribution and Velocity Are Altered in *arp2-2* Cells and Salt Stress Increases the Difference.

(A) Mitochondrial organization in roots of the wild type (WT) and *arp2-2*. Seven-day-old seedlings of transgenic wild type and *arp2-2* expressing *Pro35S*:*fABD2-GFP* were stained with MitoTracker and visualized via confocal microscopy. MF organization (top panels), mitochondrial organization (center panels), and overlay (bottom panels). White arrows point to aggregated mitochondria in the *arp2-2* mutant. At least six independent roots were analyzed in three experiments with similar results. Bar = 10 μm for all fluorescence images.

(B) Mitochondrial movement in hypocotyl cells of the wild type and *arp2-2*. Mitochondria were stained with MitoTracker (examples marked with arrowheads), and photographs were taken of hypocotyl cells from transgenic wild type and *arp2-2* expressing *Pro35S*:*fABD2-GFP*. Bar = 5 μm for all fluorescence images.

(C) Mitochondrial velocity of the wild type and *arp2-2*. Mitochondria were labeled with mitochondria-targeted cpYFP and were visualized with spinning-disc confocal microscopy. Seven-day-old seedlings of transgenic plants were treated without or with 150 mM NaCl for the indicated times. $n > 700$.

mPTPs were found in *arp2-2* than in the wild type even before salt stress, although the difference was not significant. After short (10 min) or long (4 h) exposures to salt, the percentage of cells with normal (closed) mPTP activity was dramatically decreased in *arp2-2* compared with in the wild type, being ~90 and 50% in the wild type, respectively, but only 55 and 10% in *arp2-2* (Figure 6C). To demonstrate that the calcein was localized to the mitochondria, we determined if calcein emission was decreased by the addition of tetramethyl rhodamine methyl ester (TMRM). TMRM is a cell-permeant, cationic, red-orange fluorescent dye that is readily sequestered by active mitochondria (Schwarzlander et al., 2012). As expected, addition of TMRM decreased the calcein fluorescence. The cells were then treated with carbonyl cyanide-*p*-trifluoromethoxyphenylhydrazone (FCCP), which is a chemical uncoupler of electron transport and oxidative phosphorylation. The addition of FCCP decreased the TMRM fluorescence and restored the calcein emission (see Supplemental Figure 7 online). Consistent with previous reports (Petronilli et al., 1999, 2001; Wang et al., 2010), our results demonstrate that calcein emission can be restored by FCCP uncoupling agents that cause TMRM release from mitochondria.

It has been reported that the opening of the mPTP is associated with changes in MTP (Wang et al., 2010). When we measured MTP using TMRM, wild-type cells showed a time-dependent decrease in TMRM accumulation after salt treatment. Consistent with measurements of increased mPTP opening in *arp2-2*, MTP was reduced more in the mutant compared with the wild type at all time points during salt treatment (see Supplemental Figure 6 online; Figure 6D).

To discriminate between the opening of the mPTP channel and a specific mitochondrial channel allowing influx of cations or efflux of anions, we examined the effect of NaCl treatment on matrix pH. A mitochondrial-localized, GFP-based, pH-sensitive biosensor (Orij et al., 2009) was placed under the control of the 35S promoter, and the resulting plasmid was transformed into wild-type and *arp2-2* protoplasts. The mito-pH-GFP colocalized with Mito Tracker (see Supplemental Figure 8A online), and the mitochondrial pH change was determined by a change of intensity of mito-pH-GFP (F/F_0, excitation 488 nm/excitation 405 nm) (see Supplemental Figure 8B online). Before NaCl treatment, the mitochondrial matrix pH in the *arp2-2* mutant was lower than in the wild type; after NaCl treatment, the pH decreased in both the wild type and *arp2-2* and was still lower in *arp2-2* than in the wild type. Our results suggest that both the nonspecific channel (mPTP) and specific channel (calcium channel) are affected by the *arp2* mutation.

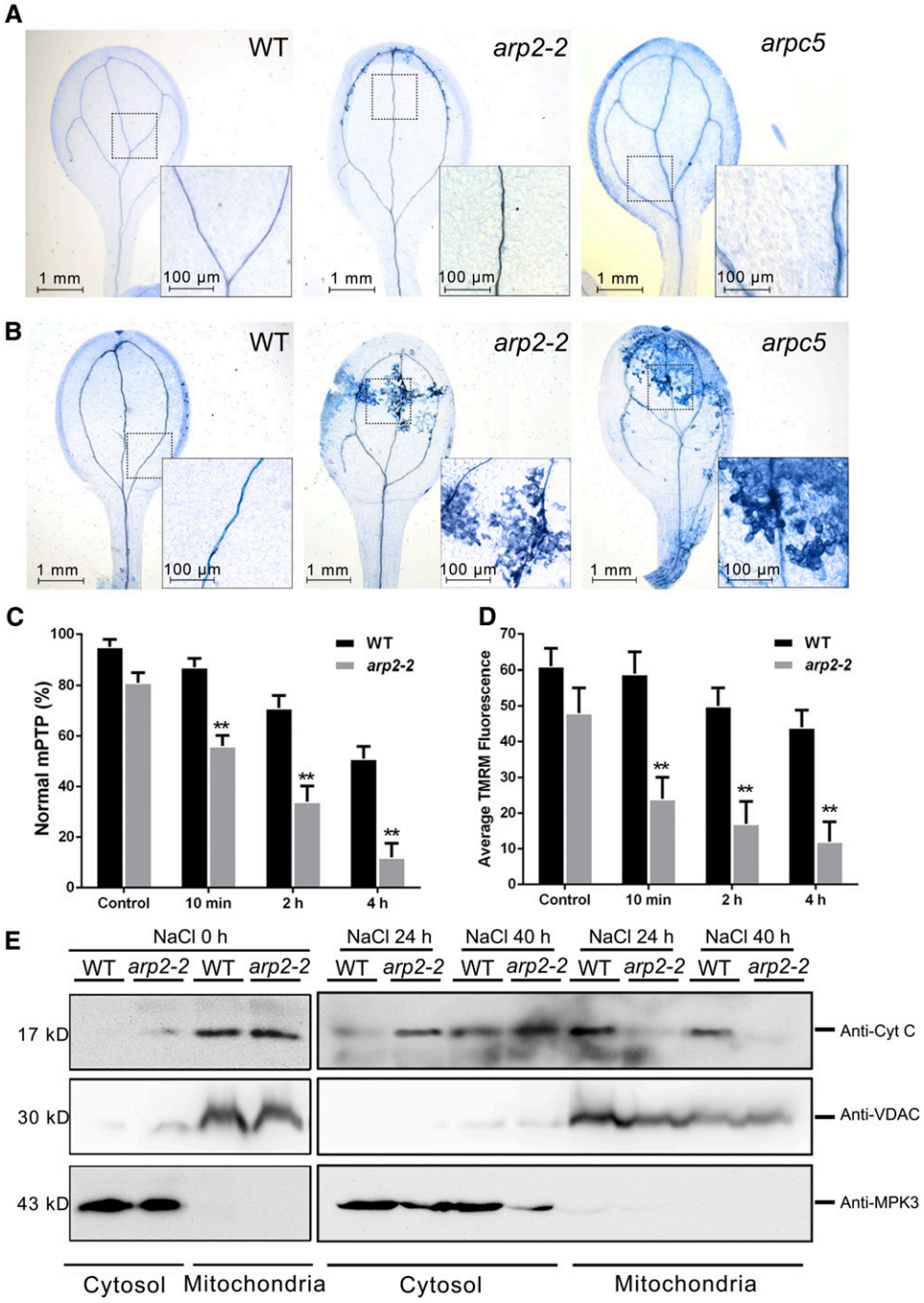

Figure 6. Salt Stress Induces Cell Death and Permeability of the Mitochondrial Membrane in *arp2-2*.

(A) Vital staining of cotyledons of the wild type (WT), *arp2-2*, and *arpc5* grown in the absence of salt. Five-day-old seedlings were stained with trypan blue. At least six independent leaves were analyzed in two experiments with similar results. Insets show enlarged views of the boxed regions.

(B) Vital staining of cotyledons of the wild type, *arp2-2*, and *arpc5* grown in the presence of salt. Five-day-old seedlings were treated with 150 mM NaCl for 24 h and then stained with trypan blue. At least six independent leaves were analyzed in two experiments with similar results. Insets show enlarged views of the boxed regions.

(C) Percentage of wild-type and *arp2-2* mutant cells with strong calcein fluorescence before and after salt treatment. The fluorescence of calcein indicates the mPTP opening status. Protoplasts were isolated from leaves of 18-d-old wild type and *arp2-2* and were left untreated or treated with 150 mM NaCl for 10 min or 2 or 4 h, and calcein staining was monitored. The number of cells analyzed per treatment was > 100, and error bars represent mean ± SE. **P < 0.01 by Student's *t* test.

Cytochrome *c* induces apoptosis in animals, and there is growing evidence that it has a similar function during plant cell death (Balk et al., 1999; Yao et al., 2004; Lin et al., 2005). Because the release of cytochrome *c* to the cytoplasm from the mitochondrion is a direct result of mPTP opening, we determined if there was a difference in cytochrome *c* release in *arp2-2* relative to the wild type as another measure of altered mPTP function in the mutant. An immunoblot assay was performed, and cytochrome *c* was detected in the mitochondrion before salt treatment in both the wild type and *arp2-2* (Figure 6E). A strong cytochrome *c* protein signal was detected in the cytoplasm of the *arp2-2* mutant with little protein detected in the mitochondrial fraction after 24 or 40 h of treatment with 150 mM NaCl. In the wild type, all cytochrome *c* was detected in the mitochondrion after 24 h of salt treatment, and after extended treatment (40 h), much of the cytochrome *c* signal remained in the mitochondrion (Figure 6E). These data demonstrate that the release of cytochrome *c* in *arp2-2* cells is much faster than in the wild type during salt stress.

The Enhanced $[Ca^{2+}]_{cyt}$ and Salt Sensitivity of *arp2-2* Is Associated with mPTP Opening

It has been reported that pretreatment of cells with cyclosporine A (CsA), an inhibitor of mPTP opening, slowed the decrease in MTP and reduced programmed cell death in tobacco (*Nicotiana tabacum*) protoplasts (Lin et al., 2005). To determine if the salt sensitivity of *arp2-2* is a mitochondrial-dependent process, wild-type and *arp2-2* protoplasts were pretreated with 5 μM CsA for 10 min and then treated with 150 mM NaCl for 4 h. Consistent with the previous results (Figure 6C), NaCl treatment significantly induced mPTP opening, which was more pronounced in *arp2-2*. Opening of mPTPs in *arp2-2* was significantly reduced in CsA-pretreated samples (Figures 7A and 7B). When 7-d-old seedlings were transferred to medium containing 200 mM NaCl with or without 50 μM CsA and grown for 5 d, the percentage of *arp2-2* seedlings that survived increased significantly on medium with CsA. These results demonstrate that blocking the mPTP leads to rescue of the *arp2-2* salt-sensitive phenotype and suggest that Arp2 functions in a mitochondrial-dependent process required for salt tolerance in plants (Figures 7C and 7D). Blocking mPTP opening also partially inhibited the salt-induced increase in $[Ca^{2+}]_{cyt}$ in *arp2-2*, as shown by the reduction in salt-induced $[Ca^{2+}]_{cyt}$-dependent luminescence of *arp2-2* seedlings when plants were pretreated with 2 μM CsA (Figure 7E). Consistent with this result, when wild-type and *arp2-2* seedlings were pretreated with 1 or 5 μM CsA for 0.5 h, the salt-induced increase in $[Ca^{2+}]_{cyt}$ in *arp2-2* dropped to nearly the same level as that in the wild type (Figure 7F). These data are consistent with previous studies that demonstrate that the mPTP is involved in Ca^{2+} homeostasis in plant cells (Lin et al., 2005) and demonstrate that the salt-induced increase in $[Ca^{2+}]_{cyt}$ in *arp2-2* results partly from mitochondrial Ca^{2+} stores.

When *arp2-2* plants were pretreated with La^{3+}, a nonselective Ca^{2+} channel blocker, for 10 min and transferred to MS with 200 mM NaCl, seedling salt sensitivity was partially rescued, though less so than seedlings treated with CsA (see Supplemental Figure 9 online), suggesting that an increase in $[Ca^{2+}]_{cyt}$ contributes to the salt-sensitive phenotype of the *arp2* mutant.

DISCUSSION

In addition to studies of the well-characterized Ca^{2+} signal–activated SOS pathway (Zhu, 2003; Quan et al., 2007), the importance of Ca^{2+} signaling in the response of the plant to salt stress has been demonstrated in numerous studies focused on calcium-dependent protein kinases (Mehlmer et al., 2010), calcium sensors (Magnan et al., 2008; Huh et al., 2010), and calcium transporters (Cheng et al., 2004; Anil et al., 2008; Zhao et al., 2009). Changes in $[Ca^{2+}]_{cyt}$ are perceived and transduced by these proteins to signal downstream responses. However, it has been unclear whether external Ca^{2+} stores (the apoplast) or internal stores (such as the endoplasmic reticulum, Golgi bodies, the vacuole, or mitochondria) are responsible for the $[Ca^{2+}]_{cyt}$ changes and how these stores are regulated during salt stress (Feng et al., 2013). Our results demonstrate that the salt-induced increase in $[Ca^{2+}]_{cyt}$ in *arp2-2* results partly from mitochondrial Ca^{2+} stores.

In plant cells, many extracellular stimuli trigger rapid changes in cytoskeletal organization, and these changes may serve as signals to regulate cellular responses, including programmed cell death (Wasteneys and Yang, 2004; Hussey et al., 2006; Smertenko and Franklin-Tong, 2011). Previous studies have shown that, in response to salt stress, the SOS pathway (Wang et al., 2007; Ye et al., 2013) and a pathway involving SOS3-like Calcium Binding Protein1, SOS2-like Protein Kinase5, and the plasma membrane H^+-ATPase (Fuglsang et al., 2007) involve regulation of MF organization (Liu and Guo, 2011). However, it has not been clear where in the pathway, relative to each other, changes in Ca^{2+} and cytoskeletal dynamics act. Many actin binding proteins, including villin and gelsolin, are regulated by Ca^{2+} signals to modulate MF organization and dynamics (Fu, 2010). Recently Wang et al. (2010) reported that disruption of MFs by Lat B or jasplakinolide leads to $[Ca^{2+}]_{cyt}$ increases possibly by modulating the opening of the mPTP, suggesting that MF dynamics trigger $[Ca^{2+}]_{cyt}$ changes. In this study, we show that the Arp2/3 complex functions to regulate mitochondrial-dependent changes in $[Ca^{2+}]_{cyt}$ during plant growth in response to

Figure 6. (continued).

(D) Average TMRM fluorescence in single protoplasts. TMRM florescence was measured in control cells or cells treated with 150 mM NaCl for 10 min or 2 or 4 h. The number of cells analyzed per treatment was > 100, and error bars represent mean ± SE. **P < 0.01 by Student's *t* test.

(E) Immunodetection of cytochrome *c* accumulation in mitochondrial and cytosolic fractions of leaves from wild-type and *arp2-2* seedlings grown in MS medium without or with 150 mM NaCl for 24 or 40 h. Anti-VDAC and anti-MPK3 antibodies were used as controls for cell fractionation.

[See online article for color version of this figure.]

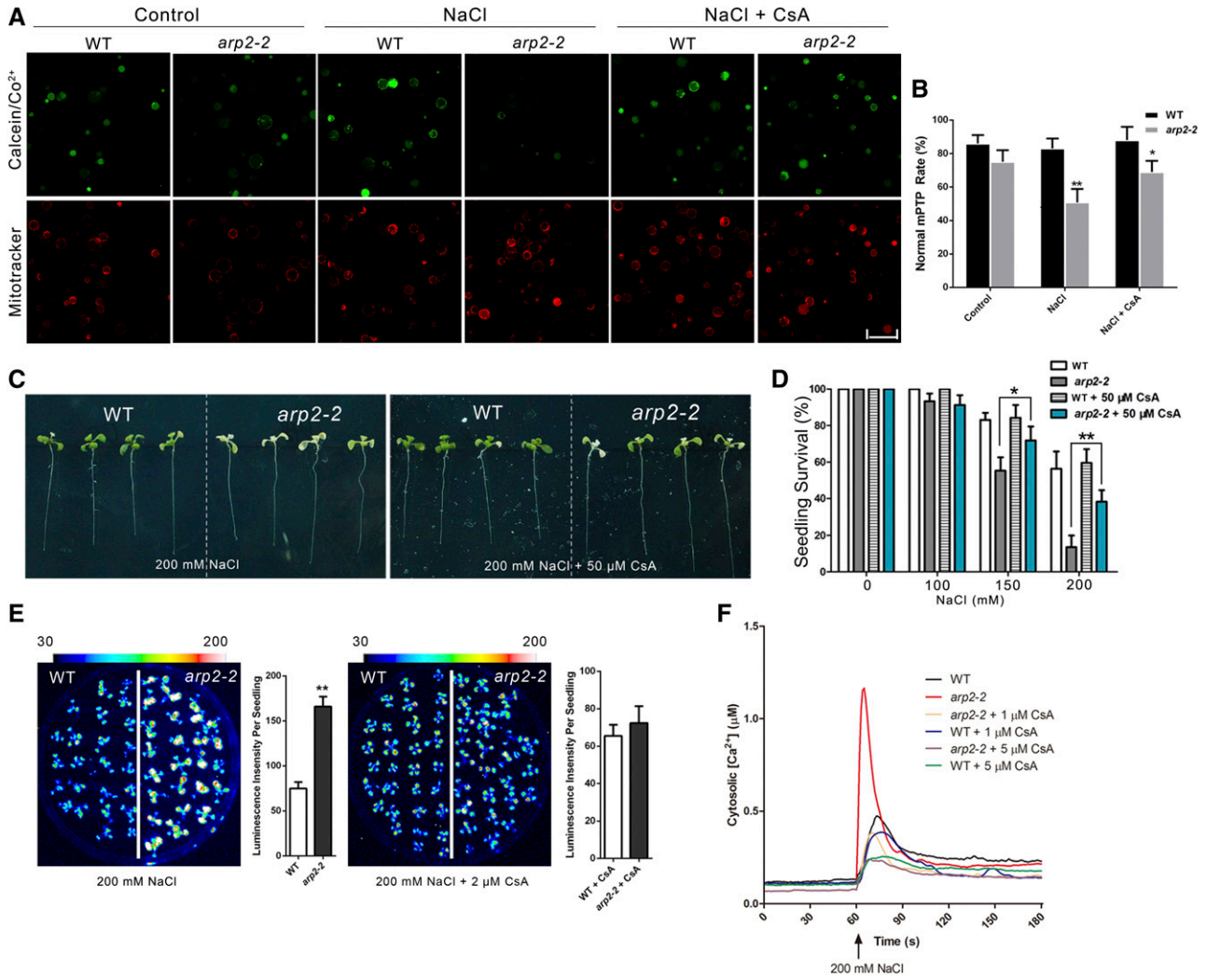

Figure 7. Blocking mPTP Opening Reverses the Salt Sensitivity and Reduces the Salt-Induced Ca^{2+} Signal in *arp2-2*.

(A) Protoplasts isolated from 18-d-old wild-type (WT) and *arp2-2* seedlings were double stained with calcein and MitoTracker in MS solution or MS solution with 150 mM NaCl with or without 10 μM CsA.

(B) Percentage of cells with normal calcein fluorescence with CsA treatment. Protoplasts were isolated from 18-d-old wild-type and *arp2-2* leaves and were left untreated or treated with 150 mM NaCl for 2 or 4 h. Protoplasts were then treated with 10 μM CsA, and calcein staining was monitored. Number of cells analyzed per treatment was > 100, and error bars represent means ± SD. Asterisks indicate a significant difference (*P < 0.05 and **P < 0.01; Student's *t* test) for *arp2-2* with and without 10 μM CsA.

(C) Seedling salt sensitivity with and without CsA. Five-day-old wild-type and *arp2-2* seedlings grown on solid MS medium were transferred to solid MS medium containing 200 mM NaCl or 200 mM NaCl with 50 μM CsA. Photographs were taken 4 d after treatment.

(D) Seedling survival for the wild type and *arp2-2* treated with salt with CsA. Five-day-old wild-type and *arp2-2* seedlings were transferred from solid MS medium to solid MS medium without or with 100, 150, or 200 mM NaCl without or with 50 μM CsA. Survival (green cotyledons and rosette leaves) was measured 4 d after transfer. Data represent means ± SD; $n > 30$. Asterisks indicate a significant difference (*P < 0.05 and **P < 0.01; Student's *t* test) for *arp2-2* with or without the addition of CsA.

(E) Pseudocolor luminescence image of Ca^{2+}-dependent photons emitted by aequorin in salt-treated (200 mM NaCl) wild-type and *arp2-2* plants without (left panel) or with 1 μM CsA (right panel). The mean luminescence value of wild-type and *arp2-2* single seedlings over a 180-s integration period is shown in the graphs to the right of the image. Data represent means ± SD; $n = 60$. Asterisks indicate a significant difference (**P < 0.01; Student's *t* test) between *arp2-2* and the wild type for the 200 mM NaCl treatment.

(F) Time course of $[Ca^{2+}]_{cyt}$ levels in 10-d-old wild-type and *arp2-2* seedlings pretreated with 1 or 5 μM CsA in response to treatment with 200 mM NaCl (arrow). The data show one representative image of five independent experiments.

salt, indicating that changes in cytoskeletal organization function upstream of changes in $[Ca^{2+}]_{cyt}$. Consistent with published results (Wang et al., 2010), disruption of MFs by Lat B treatment in the wild type increased $[Ca^{2+}]_{cyt}$; however, this treatment only slightly reduced $[Ca^{2+}]_{cyt}$ in the *arp2-2* mutant, which was much higher than $[Ca^{2+}]_{cyt}$ in the wild type treated with Lat B (see Supplemental Figure 4 online). These results suggest that the regulation of $[Ca^{2+}]_{cyt}$ change by MFs takes place at least partly through the Arp2/3 complex.

Our results demonstrate that the Arp2/3 complex is also involved in the regulation of plant growth during salt stress by modulating MF dynamics and mPTP opening. The pore regulates $[Ca^{2+}]_{cyt}$ signaling as part of a pathway required to maintain growth in salt. If, as in the *arp2-2* mutant, the pore is misregulated, $[Ca^{2+}]_{cyt}$ increases to levels that signal cell death and result in seedling salt sensitivity. Our data show that tight regulation of $[Ca^{2+}]_{cyt}$ from mitochondrial stores is critical for achieving specificity in Ca^{2+} signaling in plants.

Recently, actin proteins and actin filaments were found in mitochondria in mung bean (Lo et al., 2011), implying that MFs may play an important role in regulating the function in this organelle. In budding yeast (*Saccharomyces cerevisiae*), the Arp2/3 complex drives actin-based mitochondrial movement (Boldogh et al., 2001); Jsn1p, a Pumilo family protein, recruits the Arp2/3 complex to mitochondria (Fehrenbacher et al., 2005); and mutations in Arp2/3 complex subunits result in defects in mitochondrial morphology and movement (Fehrenbacher et al., 2004). We found that At-Arp2 possibly colocalized with mitochondria (see Supplemental Figure 5 online), suggesting that the Arp2/3 complex may be directly involved in regulating the function of mitochondria. For instance, the Arp2/3 complex may play a role in regulating the integrity of mitochondria and consequently regulate calcium release from this organelle, similar to what has been shown in budding yeast (Fehrenbacher et al., 2004, 2005). While mitochondria still move along MFs in *arp2-2* (Figure 5B), the velocity of motility was decreased substantially (Figure 5C). This suggests that Arp2/3 complex–mediated actin dynamics participate in regulating mitochondria movement but are not required for the association of mitochondria with MFs. Future studies will determine the molecular mechanism underlying Arp2/3 complex modulation of mitochondria-dependent $[Ca^{2+}]_{cyt}$ increases during salt stress and will identify the associated downstream signaling events.

METHODS

Plant Materials

Arabidopsis thaliana Col-0 constitutively expressing apoaequorin (Knight et al., 1991) was used as the wild type. Plants were grown under the intensity of 4000 lux illumination. Based on a high-throughput screening method, an enhanced $[Ca^{2+}]_{cyt}$ response mutant was isolated from a T-DNA insertion pool (pSKI015) in the wild-type background (Pan et al., 2012). Mutants of *Arp2*, *Arpc2a*, and *Arpc5* were kind gifts from Jie Le (Institute of Botany, Chinese Academic Sciences, Beijing, China).

Cytosolic Ca^{2+} Measurements

For Ca^{2+} imaging, seedlings were grown on solid MS medium with 3% Suc. Before luminescence measurements, plates of 10-d-old seedlings were sprayed with coelenterazine solution (final concentration 10 mM, 1% [v/v] ethanol, and 0.1% Triton X-100) for reconstitution. Reconstitution was allowed to proceed for a minimum of 5 h at 21°C in the dark (Knight et al., 1991). The plates were placed in the chamber of a CCD camera (Roper Scientific) after being sprayed with 200 mM NaCl or 200 mM mannitol. Photon emissions were immediately collected for 3 min. Any remaining aequorin was discharged by the addition of 1 mL of $CaCl_2$ solution (final concentration 1 M, 10% ethanol), and luminescence was collected for a further 5 min for controls. For quantitative measurements, Ca^{2+} concentration was monitored with a luminometer (GLOMAX; Promega). After aequorin reconstitution, single seedlings were pretreated as indicated and then placed in a 1.5-mL tube in the luminometer measurement chamber. Following a 60-s count for resting luminescence, 100 μL of salt solution was added automatically. Stimulated luminescence counts were recorded at 1-s intervals for 90 s. Any remaining aequorin was discharged by the addition of 200 μL of $CaCl_2$ solution (final concentration 1 M, 10% ethanol), and the counts recorded for a further 5 min until values were within 1% of the highest discharge value. The luminescence counts obtained were calibrated by applying the equation below, which takes into account the double logarithmic relationship between the concentration of free Ca^{2+} present in cells and the remaining aequorin discharged at any point in time (Rentel and Knight, 2004); $pCa = 0.332588\ (-\log k) + 5.5593$, where k = luminescence counts s^{-1} /total luminescence counts remaining. This calibration equation was determined empirically and works on the assumption that all aequorin is discharged from all cells and all emitted light is detected.

Salt Sensitivity Assay

Seeds of mutants and the wild type were sterilized in a solution containing 20% sodium hypochlorite and 0.1% Triton X-100 for 10 min, washed five times with sterilized water, and sown on solid MS medium with 0.6% Phytagel (Sigma-Aldrich). The plates were placed at 4°C for 2 d, and then the seeds were germinated vertically at 23°C, 4000 lux under continuous illumination. Four-day-old seedlings were transferred to solid MS medium with salt and other additives as described. For relative fresh weight calculations, the mean weight of 20 individual seedlings grown under control conditions was set to 100%. Relative fresh weight was calculated as the ratio of the mean weight during treatment as a function of mean weight in control conditions. To calculate the percentage of seedlings surviving, at least 50 seedlings were scored and totally bleached seedlings scored as dead.

For ion leakage assays, 7-d-old seedlings grown on solid MS plates were transferred to solid MS media containing salt as described with three replicates for each treatment. After 24 h, seedlings were carefully removed from plates, washed with deionized water, and placed in tubes containing 5 mL of deionized water. The tubes were shaken overnight, and the conductivity of the solution was measured. The tubes containing the seedlings were then autoclaved, and after the tubes cooled to room temperature, conductivities of the solutions were measured again. The percentage of electrolyte leakage was calculated as the percentage of the conductivity before versus after autoclaving.

Map-Based Cloning and Complementation

To identify the gene mutated in line *1648*, the mutant was crossed with Landsberg *erecta* wild-type plants and the F2 progeny were screened for salt tolerance. Lines with phenotypes in the F2 generation were used for further mapping of the mutated gene using specific primers for simple sequence length polymorphism markers. Mapping primers were designed using information from The Arabidopsis Information Resource database. For *arp2-2* mutant complementation, the 1170-bp *Arp2* CDS (amplified from cDNA of *Arabidopsis* Col-0 seedlings with primers 5′-CGTCTAGAATGGACAACAAAAACGTC-3′ and 5′-CGGTCGACTTAAGCTTGGCTCATTTT-3′) was

cloned into the *Xba*I and *Sal*I sites of the pCAMBIA 1300 vector. A 1502-bp genomic DNA fragment upstream of the translation start site of *Arp2* was amplified from DNA of *Arabidopsis* Col-0 seedlings with primers 5′-CGGGTACCCTGAATGAGTTAAAGACTTTC-3′ and 5′- CGTCTAGACT-TCTCCGATTTCTATAG -3′. This fragment was cloned into the *Kpn*I and *XBa*I sites of the pCAMBIA 1300 vector containing the *Arp2* CDS and *Myc* sequence. The resulting plasmid, *1300-ARP2CP*, was introduced into *Agrobacterium tumefaciens* strain GV3101 by electroporation and transformed into *arp2-2* mutants using the floral dip method (Clough and Bent, 1998).

MF Organization

Transgenic plants harboring *Pro35S:fABD2-GFP* (Wang et al., 2008) in the wild type and the *arp2-2* background were used to visualize MF dynamics. For observation of MF changes in leaves or roots during salt stress, 7-d-old seedlings were transferred to solid MS medium containing 200 mM NaCl for the indicated times. Treated or untreated seedlings were observed under a spinning disk confocal microscope equipped with a ×60 objective (numerical aperture of 1.2), and the Z-series images were acquired with the step size set at 0.5 μm. The samples were excited at 488 nm and emission was detected using a 505- to 530-nm band-pass filter. The density of actin filaments was quantified by ImageJ (http://rsbweb.nih.gov/ij/index.html; version 1.46a) as described by Higaki et al. (2010) with slight modification. First, the Z-series images were processed with the subtract background tool (rolling ball radius is 50 pixels). Individual cells were then segmented manually and actin filaments at the cell border were eliminated. The resulting images were processed by Gamma (value 1.2) and Gaussian blurring (value 0.5). Finally, images were skeletonized by the ThinLine plug-in in Image J and projected. A constant threshold was set to all images to make them binarily. Skewness and density were measured to quantify the extent of F-actin bundling and the percentage of occupancy of F-actin in cells as previously described (Higaki et al., 2010; Li et al., 2012). The bright pixel number was counted by macro hig_255counts (http://hasezawa.ib.k.u-tokyo.ac.jp/zp/Kbi/HigStomata) and then divided by cell region pixel number to yield the density of actin filaments.

Measurement of Mitochondrial Velocity

To measure the velocity of mitochondrial movement in the wild type and mutant, images of root cells of 7-d-old seedlings expressing mitochondrial-targeted yellow fluorescent protein (YFP) were obtained with a Yokogawa spinning-disk confocal microscope. An Olympus objective (×63, 1.4–numerical aperture) was used, and YFP was excited at 488 nm. Images were acquired using Andor iQ software (Andor Technology) and processed using ImageJ and Photoshop software (Adobe Systems).

Immunofluorescence Labeling Assay

Five-day-old *Arabidopsis* (Columbia ecotype) seedlings harboring *myc-Arp2* were incubated in 4% paraformaldehyde in PEM buffer (50 mM PIPES, 2 mM EGTA, and 2 mM $MgCl_2$, pH 6.9) and fixed at room temperature for 1 h. After three washes with PEM buffer, seedlings were digested by enzyme solution (1% pectinase and 1.5% cellulose in PEM buffer) at 37°C for 40 min. After another wash with PEM buffer, seedlings were put on poly-L-Lys–coated slides, smashed, fixed at −20°C, and dried. The samples were dried in a vacuum for 3 min after 1% Triton X-100 in PEM was placed on the cover slip. After a wash with PBS (137 mM NaCl, 2.7 mM KCl, 10 mM $Na_2HPO_4 \cdot 12H_2O$, and 2 mM KH_2PO_4), the samples were incubated with the mouse anti-myc antiserum, the mouse anti-AHA2 antiserum, or the rabbit anti-VDAC1 (for VOLTAGE-DEPENDENT ANION CHANNEL1) antiserum overnight at a dilution of 1:400 in 50 mM Gly in PBS buffer. After a wash with PBS buffer, the samples were incubated with fluorescein isothiocyanate–conjugated goat anti-mouse IgG (Santa Cruz Biotechnology) or Alexa Fluor-488 goat anti-rabbit IgG antibody (Life Technologies) for 3 h at a dilution of 1:400 (Binarová et al., 1993, 2000). The mitochondria were then stained with 200 nM Mitotracker Red (Michalecka et al., 2004; Guo and Crawford, 2005). Images were acquired using a Zeiss confocal microscope.

TMRM and Calcein Staining and Imaging

Protoplasts were incubated in WM buffer (308 mM mannitol, 125 mM $CaCl_2$, 5 mM KCl, and 2 mM MES, pH 5.7) and stained with 1 μM calcein/acetoxymethyl ester and 1 mM $CoCl_2$. The stained protoplast solution was then gently flattened on poly-D-Lys–coated glass slides and 10 μM TMRM (0.2 to 0.5 μL) was added before the addition of a cover slip. Pictures of calcein-stained protoplasts were taken immediately with a fluorescence microscope (Zeiss). The calcein and TMRM signals were then recorded in fluorescent channels after 1 or 2 min. FCCP buffer (2 μM) was added by placing a drop on the edge of the cover glass to allow the solution to wick up by capillary action. Photographs were taken after 1 or 2 min.

mPTP and Mitochondria Membrane Potential Measurements

Opening of the mPTP was monitored using calcein/Co^{2+} imaging (Petronilli et al., 1999). *Arabidopsis* mesophyll protoplasts were prepared as described (Sheen, 2001). Protoplasts were placed in Wash buffer 5 (W5) buffer (154 mM NaCl, 125 mM $CaCl_2$, 5 mM KCl, and 2 mM MES, pH 5.7) or WM buffer (308 mM mannitol, 125 mM $CaCl_2$, 5 mM KCl, and 2 mM MES, pH 5.7) for the indicated times and then double-stained with 1 μM calcein/acetoxymethyl ester and 200 nM Mitotracker (Invitrogen) for 15 min before washing. For quenching of cytosolic calcein fluorescence, 1 mM $CoCl_2$ was also present during calcein loading. All staining was performed with 154 mM NaCl in W5 buffer. Stained protoplasts were placed on poly-D-Lys–coated glass slides and images were taken with a confocal microscope with a ×63 (numerical aperture of 1.4) oil objective. Calcein and Mitotracker signals were visualized with excitation at 488 nm (emission 498 to 532 nm) and 543 nm (emission 495 to 635 nm), respectively, and chloroplast autofluorescence (488 nm excitation) was visualized at 738 to 793 nm. The percentage of cells with obvious mitochondrial calcein fluorescence was calculated.

For measurements of membrane potential, 200 nM TMRM (Molecular Probes) was added to protoplasts after the indicated period of W5 treatment. The protoplasts were then incubated for 1 to 2 min at 25°C and observed with a confocal microscope with optical filters (543-nm excitation and 585-nm emission) to visualize the red fluorescent probe. Quantitative images were captured and data were analyzed using Leica software.

pH Measurement

A mitochondrial-localized, GFP-based, pH-sensitive biosensor (Orij et al., 2009) was placed under the control of the 35S promoter. The *Pro35S*:mito-pH-GFP plasmid was purified by CsCl gradient centrifugation and then was transformed into protoplasts (Sheen, 2001). Protoplasts were incubated in W5 buffer (154 mM NaCl, 125 mM $CaCl_2$, 5 mM KCl, and 2 mM MES, pH 5.7) or WM buffer (308 mM mannitol, 125 mM $CaCl_2$, 5 mM KCl, and 2 mM MES, pH 5.7) overnight at 23°C. The protoplasts were stained with 200 nM Mitotracker (Invitrogen) for 15 min before visualization using a confocal microscope. Lasers (405 and 488 nm) were used to excite the protoplasts, and the fluorescence was collected at 505 to 545 nm. The intensity level was analyzed with ImageJ software (http://rsb.info.nih.gov/ij/).

Histochemical Staining and Detection of Cytochrome *c* Release

To visualize cell death, 5-d-old seedlings were treated with 150 mM NaCl for 24 h and then stained with lactophenol trypan blue as described (Van

Wees, 2008). To detect cytochrome *c* release, 7-d-old seedlings of the wild type and *arp2-2* were treated with 200 mM NaCl for the indicated times, and control and salt-treated seedlings (0.5 g) were ground in homogenization buffer (0.4 M mannitol, 1 mM EGTA, 20 mM 2-mercaptoethanol, 50 mM Tricine, and 0.1% BSA, pH 7.8) for 1 min at 4°C. Extracts were filtered through Miracloth, and the filtrates were centrifuged at 15,000*g* for 5 min at 4°C. The supernatant was centrifuged at 16,000*g* for 15 min at 4°C. After centrifugation, the cytosolic fraction (supernatant) was collected and the mitochondrial fraction (pellet) was resuspended in homogenization buffer. Immunoblot analysis was performed as described (Kim et al., 2006). Separated proteins were transferred to polyvinylidene difluoride membranes and probed with a monoclonal antibody against cytochrome *c* (1:100 dilution; Beyotime) and a monoclonal antibody (31HL) against the *Arabidopsis* VDAC1 (Calbiochem; 1:1000 dilution). Antibody binding was detected using horseradish peroxidase–conjugated secondary antibodies (1:400 dilution) and enhanced chemiluminescence (Amersham Pharmacia Biotech).

Accession Numbers

Sequence data from this article can be found in the Arabidopsis Genome Initiative or GenBank/EMBL databases under the following accession numbers: At3g27000 (ARP2), At1g30825 (ARPC2A), and At4g01710 (ARPC5).

Supplemental Data

The following materials are available in the online version of this article.

Supplemental Figure 1. *1648* Is Sensitive to Ionic but Not Osmotic Stress.

Supplemental Figure 2. *arpc2a* Seedlings Are Hypersensitive to Salt.

Supplemental Figure 3. Salt Induces Increases in $[Ca^{2+}]_{cyt}$-Dependent Luminescence in *arp2-1*, *arpc2a*, and *arpc5* Seedlings.

Supplemental Figure 4. Depolymerization of Microfilaments Enhances Salt-Induced Increases in $[Ca^{2+}]_{cyt}$.

Supplemental Figure 5. Immunological Detection of the Arp2 Protein.

Supplemental Figure 6. Confocal Images of mPTP Function and MTP Measurements in Protoplasts.

Supplemental Figure 7. A Control Experiment to Demonstrate Calcein Is Localized to Mitochondria.

Supplemental Figure 8. Analysis of Mitochondrial Matrix pH in the Wild Type and *arp2-2*.

Supplemental Figure 9. The Salt Sensitivity of *arp2-2* Is Partially Rescued by a Ca^{2+} Channel Blocker.

ACKNOWLEDGMENTS

We thank Joerg Kudla and Tong-lin Mao for stimulating discussions and technical help. This work was supported by the National Basic Research Program of China (Grant 2012CB114200 to Y.G. and M.Y.), China National Funds for Distinguished Young Scientists (Grant 31025003 to Y.G. and Grant 31125004 to S.H.), the Natural Science Foundation of China international collaborative research project (Grant 31210103903 to Y.G.), the Foundation for Innovative Research Group of the National Natural Science Foundation of China (Grant 31121002), the National Transgenic Research Project (Grants 2013ZX08009002), and the Scholarship Award for Excellent Doctoral Student granted by Ministry of Education, China (2012) to Y.Z.

AUTHOR CONTRIBUTIONS

Y.G., Yi Z., and Z.P. designed the research. Yi Z., Z.P., Yan Z., X.Q., Yu Z., and Y.Y. performed research. X.J. contributed new analytic tools. Y.G., K.S.S., Yi Z., Z.P., S.H., and M.Y. analyzed data and wrote the article.

Received August 26, 2013; revised October 30, 2013; accepted November 14, 2013; published November 26, 2013.

REFERENCES

Anil, V.S., Rajkumar, P., Kumar, P., and Mathew, M.K. (2008). A plant Ca^{2+} pump, ACA2, relieves salt hypersensitivity in yeast. Modulation of cytosolic calcium signature and activation of adaptive Na+ homeostasis. J. Biol. Chem. **283:** 3497–3506.

Balk, J., Leaver, C.J., and McCabe, P.F. (1999). Translocation of cytochrome c from the mitochondria to the cytosol occurs during heat-induced programmed cell death in cucumber plants. FEBS Lett. **463:** 151–154.

Berridge, M.J., Bootman, M.D., and Roderick, H.L. (2003). Calcium signalling: Dynamics, homeostasis and remodelling. Nat. Rev. Mol. Cell Biol. **4:** 517–529.

Binarová, P., Cihaliková, J., and Dolezel, J. (1993). Localization of MPM-2 recognized phosphoproteins and tubulin during cell cycle progression in synchronized *Vicia faba* root meristem cells. Cell Biol. Int. **17:** 847–856.

Binarová, P., Cenklová, V., Hause, B., Kubátová, E., Lysák, M., Dolezel, J., Bögre, L., and Dráber, P. (2000). Nuclear γ-tubulin during acentriolar plant mitosis. Plant Cell **12:** 433–442.

Boldogh, I.R., Yang, H.C., Nowakowski, W.D., Karmon, S.L., Hays, L.G., Yates, J.R., III., and Pon, L.A. (2001). Arp2/3 complex and actin dynamics are required for actin-based mitochondrial motility in yeast. Proc. Natl. Acad. Sci. USA **98:** 3162–3167.

Cheng, N.H., Pittman, J.K., Zhu, J.K., and Hirschi, K.D. (2004). The protein kinase SOS2 activates the *Arabidopsis* H^+/Ca^{2+} antiporter CAX1 to integrate calcium transport and salt tolerance. J. Biol. Chem. **279:** 2922–2926.

Clough, S.J., and Bent, A.F. (1998). Floral dip: A simplified method for *Agrobacterium*-mediated transformation of *Arabidopsis thaliana*. Plant J. **16:** 735–743.

Deeks, M.J., and Hussey, P.J. (2005). Arp2/3 and SCAR: plants move to the fore. Nat. Rev. Mol. Cell Biol. **6:** 954–964.

Dyachok, J., Shao, M.R., Vaughn, K., Bowling, A., Facette, M., Djakovic, S., Clark, L., and Smith, L. (2008). Plasma membrane-associated SCAR complex subunits promote cortical F-actin accumulation and normal growth characteristics in *Arabidopsis* roots. Mol. Plant **1:** 990–1006.

Dyachok, J., Zhu, L., Liao, F., He, J., Huq, E., and Blancaflor, E.B. (2011). SCAR mediates light-induced root elongation in *Arabidopsis* through photoreceptors and proteasomes. Plant Cell **23:** 3610–3626.

Fehrenbacher, K.L., Boldogh, I.R., and Pon, L.A. (2005). A role for Jsn1p in recruiting the Arp2/3 complex to mitochondria in budding yeast. Mol. Biol. Cell **16:** 5094–5102.

Fehrenbacher, K.L., Yang, H.C., Gay, A.C., Huckaba, T.M., and Pon, L.A. (2004). Live cell imaging of mitochondrial movement along actin cables in budding yeast. Curr. Biol. **14:** 1996–2004.

Feng, S., Li, H., Tai, Y., Huang, J., Su, Y., Abramowitz, J., Zhu, M.X., Birnbaumer, L., and Wang, Y. (2013). Canonical transient receptor potential 3 channels regulate mitochondrial calcium uptake. Proc. Natl. Acad. Sci. USA **110:** 11011–11016.

Frohnmeyer, H., Loyall, L., Blatt, M.R., and Grabov, A. (1999). Millisecond UV-B irradiation evokes prolonged elevation of cytosolic-free Ca^{2+} and

stimulates gene expression in transgenic parsley cell cultures. Plant J. **20:** 109–117.

Fu, Y. (2010). The actin cytoskeleton and signaling network during pollen tube tip growth. J. Integr. Plant Biol. **52:** 131–137.

Fuglsang, A.T., Guo, Y., Cuin, T.A., Qiu, Q., Song, C., Kristiansen, K.A., Bych, K., Schulz, A., Shabala, S., Schumaker, K.S., Palmgren, M.G., and Zhu, J.K. (2007). *Arabidopsis* protein kinase PKS5 inhibits the plasma membrane H^+ -ATPase by preventing interaction with 14-3-3 protein. Plant Cell **19:** 1617–1634.

Gao, C., Xing, D., Li, L., and Zhang, L. (2008). Implication of reactive oxygen species and mitochondrial dysfunction in the early stages of plant programmed cell death induced by ultraviolet-C overexposure. Planta **227:** 755–767.

Goley, E.D., and Welch, M.D. (2006). The ARP2/3 complex: An actin nucleator comes of age. Nat. Rev. Mol. Cell Biol. **7:** 713–726.

Green, D.R., and Kroemer, G. (2004). The pathophysiology of mitochondrial cell death. Science **305:** 626–629.

Guo, F.Q., and Crawford, N.M. (2005). *Arabidopsis* nitric oxide synthase1 is targeted to mitochondria and protects against oxidative damage and dark-induced senescence. Plant Cell **17:** 3436–3450.

Guo, Y., Halfter, U., Ishitani, M., and Zhu, J.K. (2001). Molecular characterization of functional domains in the protein kinase SOS2 that is required for plant salt tolerance. Plant Cell **13:** 1383–1400.

Higaki, T., Kutsuna, N., Sano, T., Kondo, N., and Hasezawa, S. (2010). Quantification and cluster analysis of actin cytoskeletal structures in plant cells: Role of actin bundling in stomatal movement during diurnal cycles in *Arabidopsis* guard cells. Plant J. **61:** 156–165.

Huh, S.M., Noh, E.K., Kim, H.G., Jeon, B.W., Bae, K., Hu, H.C., Kwak, J.M., and Park, O.K. (2010). *Arabidopsis* annexins AnnAt1 and AnnAt4 interact with each other and regulate drought and salt stress responses. Plant Cell Physiol. **51:** 1499–1514.

Hussey, P.J., Ketelaar, T., and Deeks, M.J. (2006). Control of the actin cytoskeleton in plant cell growth. Annu. Rev. Plant Biol. **57:** 109–125.

Ishitani, M., Liu, J., Halfter, U., Kim, C.S., Shi, W., and Zhu, J.-K. (2000). SOS3 function in plant salt tolerance requires N-myristoylation and calcium binding. Plant Cell **12:** 1667–1678.

Jiang, K., Sorefan, K., Deeks, M.J., Bevan, M.W., Hussey, P.J., and Hetherington, A.M. (2012). The ARP2/3 complex mediates guard cell actin reorganization and stomatal movement in *Arabidopsis*. Plant Cell **24:** 2031–2040.

Kim, M., Lim, J.H., Ahn, C.S., Park, K., Kim, G.T., Kim, W.T., and Pai, H.S. (2006). Mitochondria-associated hexokinases play a role in the control of programmed cell death in *Nicotiana benthamiana*. Plant Cell **18:** 2341–2355.

Knight, H., Trewavas, A.J., and Knight, M.R. (1996). Cold calcium signaling in *Arabidopsis* involves two cellular pools and a change in calcium signature after acclimation. Plant Cell **8:** 489–503.

Knight, H., Trewavas, A.J., and Knight, M.R. (1997). Calcium signalling in *Arabidopsis thaliana* responding to drought and salinity. Plant J. **12:** 1067–1078.

Knight, M.R., Campbell, A.K., Smith, S.M., and Trewavas, A.J. (1991). Transgenic plant aequorin reports the effects of touch and cold-shock and elicitors on cytoplasmic calcium. Nature **352:** 524–526.

Kotchoni, S.O., Zakharova, T., Mallery, E.L., Le, J., El-Assal, Sel.-D., and Szymanski, D.B. (2009). The association of the Arabidopsis actin-related protein2/3 complex with cell membranes is linked to its assembly status but not its activation. Plant Physiol. **151:** 2095–2109.

Le, J., El-Assal, Sel.-D., Basu, D., Saad, M.E., and Szymanski, D.B. (2003). Requirements for *Arabidopsis* ATARP2 and ATARP3 during epidermal development. Curr. Biol. **13:** 1341–1347.

Li, J., Henty-Ridilla, J.L., Huang, S., Wang, X., Blanchoin, L., and Staiger, C.J. (2012). Capping protein modulates the dynamic behavior of actin filaments in response to phosphatidic acid in *Arabidopsis*. Plant Cell **24:** 3742–3754.

Lin, J., Wang, Y., and Wang, G. (2005). Salt stress-induced programmed cell death via Ca^{2+}-mediated mitochondrial permeability transition in tobacco protoplasts. Plant Growth Regul. **45:** 243–250.

Liu, J., and Guo, Y. (2011). The alkaline tolerance in *Arabidopsis* requires stabilizing microfilament partially through inactivation of PKS5 kinase. J. Genet. Genomics **38:** 307–313.

Liu, J., Ishitani, M., Halfter, U., Kim, C.S., and Zhu, J.K. (2000). The *Arabidopsis thaliana* SOS2 gene encodes a protein kinase that is required for salt tolerance. Proc. Natl. Acad. Sci. USA **97:** 3730–3734.

Liu, J., and Zhu, J.K. (1998). A calcium sensor homolog required for plant salt tolerance. Science **280:** 1943–1945.

Lo, Y.S., Cheng, N., Hsiao, L.J., Annamalai, A., Jauh, G.Y., Wen, T.N., Dai, H., and Chiang, K.S. (2011). Actin in mung bean mitochondria and implications for its function. Plant Cell **23:** 3727–3744.

Machesky, L.M., and Gould, K.L. (1999). The Arp2/3 complex: A multifunctional actin organizer. Curr. Opin. Cell Biol. **11:** 117–121.

Magnan, F., Ranty, B., Charpenteau, M., Sotta, B., Galaud, J.P., and Aldon, D. (2008). Mutations in AtCML9, a calmodulin-like protein from *Arabidopsis thaliana*, alter plant responses to abiotic stress and abscisic acid. Plant J. **56:** 575–589.

Mathur, J. (2005). The ARP2/3 complex: Giving plant cells a leading edge. Bioessays **27:** 377–387.

Mathur, J., Spielhofer, P., Kost, B., and Chua, N. (1999). The actin cytoskeleton is required to elaborate and maintain spatial patterning during trichome cell morphogenesis in *Arabidopsis thaliana*. Development **126:** 5559–5568.

Mehlmer, N., Wurzinger, B., Stael, S., Hofmann-Rodrigues, D., Csaszar, E., Pfister, B., Bayer, R., and Teige, M. (2010). The $Ca^{(2+)}$-dependent protein kinase CPK3 is required for MAPK-independent salt-stress acclimation in *Arabidopsis*. Plant J. **63:** 484–498.

Michalecka, A.M., Agius, S.C., Møller, I.M., and Rasmusson, A.G. (2004). Identification of a mitochondrial external NADPH dehydrogenase by overexpression in transgenic *Nicotiana sylvestris*. Plant J. **37:** 415–425.

Orij, R., Postmus, J., Ter Beek, A., Brul, S., and Smits, G.J. (2009). In vivo measurement of cytosolic and mitochondrial pH using a pH-sensitive GFP derivative in Saccharomyces cerevisiae reveals a relation between intracellular pH and growth. Microbiology **155:** 268–278.

Pan, Z., Zhao, Y., Zheng, Y., Liu, J., Jiang, X., and Guo, Y. (2012). A high-throughput method for screening *Arabidopsis* mutants with disordered abiotic stress-induced calcium signal. J. Genet. Genomics **39:** 225–235.

Petronilli, V., Miotto, G., Canton, M., Brini, M., Colonna, R., Bernardi, P., and Di Lisa, F. (1999). Transient and long-lasting openings of the mitochondrial permeability transition pore can be monitored directly in intact cells by changes in mitochondrial calcein fluorescence. Biophys. J. **76:** 725–734.

Petronilli, V., Penzo, D., Scorrano, L., Bernardi, P., and Di Lisa, F. (2001). The mitochondrial permeability transition, release of cytochrome c and cell death. Correlation with the duration of pore openings in situ. J. Biol. Chem. **276:** 12030–12034.

Qiu, Q.S., Barkla, B.J., Vera-Estrella, R., Zhu, J.K., and Schumaker, K.S. (2003). Na^+/H^+ exchange activity in the plasma membrane of Arabidopsis. Plant Physiol. **132:** 1041–1052.

Qiu, Q.S., Guo, Y., Dietrich, M.A., Schumaker, K.S., and Zhu, J.K. (2002). Regulation of SOS1, a plasma membrane Na^+/H^+ exchanger in *Arabidopsis thaliana*, by SOS2 and SOS3. Proc. Natl. Acad. Sci. USA **99:** 8436–8441.

Quan, R., Lin, H., Mendoza, I., Zhang, Y., Cao, W., Yang, Y., Shang, M., Chen, S., Pardo, J.M., and Guo, Y. (2007). SCABP8/CBL10, a putative calcium sensor, interacts with the protein kinase SOS2 to protect *Arabidopsis* shoots from salt stress. Plant Cell **19:** 1415–1431.

Rentel, M.C., and Knight, M.R. (2004). Oxidative stress-induced calcium signaling in Arabidopsis. Plant Physiol. **135:** 1471–1479.

Schwarzländer, M., Logan, D.C., Johnston, I.G., Jones, N.S., Meyer, A.J., Fricker, M.D., and Sweetlove, L.J. (2012). Pulsing of membrane potential in individual mitochondria: A stress-induced mechanism to regulate respiratory bioenergetics in *Arabidopsis*. Plant Cell **24:** 1188–1201.

Sheen, J. (2001). Signal transduction in maize and Arabidopsis mesophyll protoplasts. Plant Physiol. **127:** 1466–1475.

Shi, H., Ishitani, M., Kim, C., and Zhu, J.K. (2000). The *Arabidopsis thaliana* salt tolerance gene SOS1 encodes a putative Na^+/H^+ antiporter. Proc. Natl. Acad. Sci. USA **97:** 6896–6901.

Smertenko, A., and Franklin-Tong, V.E. (2011). Organisation and regulation of the cytoskeleton in plant programmed cell death. Cell Death Differ. **18:** 1263–1270.

Szymanski, D.B. (2005). Breaking the WAVE complex: The point of *Arabidopsis* trichomes. Curr. Opin. Plant Biol. **8:** 103–112.

Vandecasteele, G., Szabadkai, G., and Rizzuto, R. (2001). Mitochondrial calcium homeostasis: Mechanisms and molecules. IUBMB Life **52:** 213–219.

van Wees, S. (2008). Phenotypic analysis of *Arabidopsis* mutants: Trypan blue stain for fungi, oomycetes, and dead plant cells. CSH Protoc **2008:** t4982.

Wang, C., Li, J., and Yuan, M. (2007). Salt tolerance requires cortical microtubule reorganization in *Arabidopsis*. Plant Cell Physiol. **48:** 1534–1547.

Wang, Y., Zhu, Y., Ling, Y., Zhang, H., Liu, P., Baluska, F., Samaj, J., Lin, J., and Wang, Q. (2010). Disruption of actin filaments induces mitochondrial Ca^{2+} release to the cytoplasm and $[Ca^{2+}]_c$ changes in *Arabidopsis* root hairs. BMC Plant Biol. **10:** 53.

Wang, Y.F., Fan, L.-M., Zhang, W.Z., Zhang, W., and Wu, W.H. (2004a). Ca^{2+}-permeable channels in the plasma membrane of Arabidopsis pollen are regulated by actin microfilaments. Plant Physiol. **136:** 3892–3904.

Wang, Y.S., Motes, C.M., Mohamalawari, D.R., and Blancaflor, E.B. (2004b). Green fluorescent protein fusions to *Arabidopsis* fimbrin 1 for spatio-temporal imaging of F-actin dynamics in roots. Cell Motil. Cytoskeleton **59:** 79–93.

Wang, Y.S., Yoo, C.M., and Blancaflor, E.B. (2008). Improved imaging of actin filaments in transgenic *Arabidopsis* plants expressing a green fluorescent protein fusion to the C- and N-termini of the fimbrin actin-binding domain 2. New Phytol. **177:** 525–536.

Wasteneys, G.O., and Yang, Z. (2004). New views on the plant cytoskeleton. Plant Physiol. **136:** 3884–3891.

Wojtera-Kwiczor, J., Groß, F., Leffers, H.M., Kang, M., Schneider, M., and Scheibe, R. (2012). Transfer of a redox-signal through the cytosol by redox-dependent microcompartmentation of glycolytic enzymes at mitochondria and actin cytoskeleton. Front. Plant Sci. **3:** 284.

Yanagisawa, M., Zhang, C.H., and Szymanski, D.B. (2013). ARP2/3-dependent growth in the plant kingdom: SCARs for life. Front. Plant Sci. **4:** 166.

Yang, J., Liu, X., Bhalla, K., Kim, C.N., Ibrado, A.M., Cai, J., Peng, T.I., Jones, D.P., and Wang, X. (1997). Prevention of apoptosis by Bcl-2: Release of cytochrome c from mitochondria blocked. Science **275:** 1129–1132.

Yao, N., Eisfelder, B.J., Marvin, J., and Greenberg, J.T. (2004). The mitochondrion—An organelle commonly involved in programmed cell death in *Arabidopsis thaliana*. Plant J. **40:** 596–610.

Ye, J., Zhang, W., and Guo, Y. (2013). *Arabidopsis* SOS3 plays an important role in salt tolerance by mediating calcium-dependent microfilament reorganization. Plant Cell Rep. **32:** 139–148.

Zhang, C., Mallery, E., Reagan, S., Boyko, V.P., Kotchoni, S.O., and Szymanski, D.B. (2013). The endoplasmic reticulum is a reservoir for WAVE/SCAR regulatory complex signaling in the Arabidopsis leaf. Plant Physiol. **162:** 689–706.

Zhao, J., Connorton, J.M., Guo, Y., Li, X., Shigaki, T., Hirschi, K.D., and Pittman, J.K. (2009). Functional studies of split *Arabidopsis* Ca^{2+}/H^+ exchangers. J. Biol. Chem. **284:** 34075–34083.

Zhao, Y., Christensen, S.K., Fankhauser, C., Cashman, J.R., Cohen, J.D., Weigel, D., and Chory, J. (2001). A role for flavin monooxygenase-like enzymes in auxin biosynthesis. Science **291:** 306–309.

Zhao, Y., et al. (2011). The plant-specific actin binding protein SCAB1 stabilizes actin filaments and regulates stomatal movement in *Arabidopsis*. Plant Cell **23:** 2314–2330.

Zheng, M.Z., Beck, M., Müller, J., Chen, T., Wang, X.H., Wang, F., Wang, Q.L., Wang, Y.Q., Baluska, F., Logan, D.C., Samaj, J., and Lin, J.X. (2009). Actin turnover is required for myosin-dependent mitochondrial movements in *Arabidopsis* root hairs. PLoS One **4:** e5961.

Zheng, Y., Schumaker, K.S., and Guo, Y. (2012). Sumoylation of transcription factor MYB30 by the small ubiquitin-like modifier E3 ligase SIZ1 mediates abscisic acid response in *Arabidopsis thaliana*. Proc. Natl. Acad. Sci. USA **109:** 12822–12827.

Zhou, Y., Yang, Z., Guo, G., and Guo, Y. (2010). Microfilament dynamics is required for root growth under alkaline stress in *Arabidopsis*. J. Integr. Plant Biol. **52:** 952–958.

Zhu, J.K. (2003). Regulation of ion homeostasis under salt stress. Curr. Opin. Plant Biol. **6:** 441–445.

Zhu, J.K., Liu, J., and Xiong, L. (1998). Genetic analysis of salt tolerance in *Arabidopsis*. Evidence for a critical role of potassium nutrition. Plant Cell **10:** 1181–1191.

The Actin-Related Protein2/3 Complex Regulates Mitochondrial-Associated Calcium Signaling during Salt Stress in *Arabidopsis*

Yi Zhao, Zhen Pan, Yan Zhang, Xiaolu Qu, Yuguo Zhang, Yongqing Yang, Xiangning Jiang, Shanjin Huang, Ming Yuan, Karen S. Schumaker and Yan Guo

Plant Cell 2013;25;4544-4559; originally published online November 26, 2013;
DOI 10.1105/tpc.113.117887

This information is current as of February 12, 2014

Supplemental Data	**http://www.plantcell.org/content/suppl/2013/11/20/tpc.113.117887.DC1.html**
References	This article cites 80 articles, 42 of which can be accessed free at: http://www.plantcell.org/content/25/11/4544.full.html#ref-list-1
Permissions	https://www.copyright.com/ccc/openurl.do?sid=pd_hw1532298X&issn=1532298X&WT.mc_id=pd_hw1532298X
eTOCs	Sign up for eTOCs at: http://www.plantcell.org/cgi/alerts/ctmain
CiteTrack Alerts	Sign up for CiteTrack Alerts at: http://www.plantcell.org/cgi/alerts/ctmain
Subscription Information	Subscription Information for *The Plant Cell* and *Plant Physiology* is available at: http://www.aspb.org/publications/subscriptions.cfm

© American Society of Plant Biologists

ADVANCING THE SCIENCE OF PLANT BIOLOGY